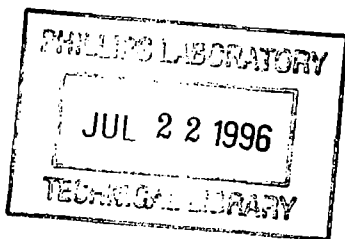


Library for Phillips  
11 Jun 96  
PL 96-0422

Sensor and Simulation Notes



Note 395

April 1996

**Coaxial Beam-Rotating Antenna (COBRA) Concepts**

**Clifton C. Courtney**  
*Voss Scientific*

**Carl E. Baum**  
*Phillips Laboratory / WSQ*

**Abstract**

Many high power microwave (HPM) sources utilize the  $TM_{01}$  ( $E_{01}$ ) circular waveguide, or the coaxial TEM mode as the output mode. If radiated directly, these modes generate a doughnut-shaped radiation pattern with a boresight null. Mode conversion techniques and antenna designs have been explored to remedy this shortcoming, but mode conversion is not perfect (efficiencies are typically 50% to 75%), and the antenna designs considered to date tend to be low gain, and do not radiate a boresight peak (along the axis of the source). This paper describes a concept for a novel class of reflector antennas. Designated the Coaxial Beam-Rotating Antenna (COBRA), these antennas accept directly the guided mode of the source and radiate a high gain, circularly polarized, pencil beam boresight peak. Various configurations of the COBRA concept will be presented including: single, stepped paraboloidal reflector; dual reflector with stepped subreflector; and configurations with coaxial feeds that drive directly the reflector / subreflector.

## 1.0 Introduction

Many high power microwave (HPM) electromagnetic sources utilize the  $TM_{01}$  circular waveguide or TEM coaxial modes as the output mode. For example, some MILO-type HPM sources generate RF energy in coaxial geometries. RF extraction then is made by converting the coaxial TEM mode to a  $TM_{01}$  circular waveguide mode. If radiated directly, these non-standard modes generate a doughnut-shaped pattern with a “target cone of protection” null-on boresight. To avoid this, one often resorts to mode conversion techniques to change the coaxial TEM or circular  $TM_{01}$  mode to more useful ones, such as circular  $TE_{11}$  or rectangular  $TE_{01}$ . The radiation patterns of these modes exhibit a peak-on boresight. Unfortunately, mode conversion is not perfect (conversion efficiencies of between 50% and 75% are typical), and the addition of the mode converter adds weight and length to the source. Other antenna designs have been considered, but they do not radiate a pattern peak along the axis of the source (consequently the nature in which the HPM is pointed becomes an issue), and exhibit low to moderate gain characteristics. They also radiate linear polarization, which in some instances is a liability since coupling to the aperture(s) of a target can be polarization dependent (the circular polarization of the radiated field of the COBRA also could be a disadvantage if the intended coupling mechanism is via a circularly polarized antenna with the opposite sense).

This paper will discuss ways to convert the less useful modes described above into more useful ones. The antenna designs resulting from these considerations have been named Coaxial Beam-Rotating Antennas (COBRA). These antennas accept directly the guided mode of the source and radiate a high gain, circularly polarized, pencil-beam boresight peak field. Circular polarization, while sacrificing peak electric field for a given power density, increases the probability that the target is exposed to the optimal coupling polarization, provided

the coupling is approximately linearly polarized. Also, since it is shared by the orthogonal polarizations, the maximum power density one can realize before air breakdown occurs is greater with a circularly polarized field than that achievable with a linearly polarized field. Additionally, the antennas associated with the COBRA concepts discussed here can attach directly to the end of an HPM source with coaxial or circular waveguide output, and radiate a pattern peak along the axial direction of the source. Preliminary conservative computations indicate that the COBRA will exhibit boresight circular polarization with a gain for each polarization component that is -6.9 dB (for a four-step reflector, asymptotically better for an increased number of steps) below that of a uniformly filled, linearly polarized aperture.

The next section presents a discussion of the characteristics of circular polarization. This is followed by Section 3, which is concerned with the fundamental concepts of operation common to all COBRA geometries, and gives an estimate of the radiated field and gain of a simple COBRA configuration with a four-step reflector. In Section 4, other COBRA geometries are illustrated, including: single, stepped paraboloidal reflector; dual reflector with stepped subreflector; and configurations with coaxial feeds that directly drive the reflector / subreflector. The final section presents some concluding remarks, and discusses the direction of future efforts in this area. An appendix is presented that computes the radiated field of the COBRA aperture for the general case of  $N$  steps, computes the radiated field of a linearly polarized, uniformly illuminated aperture, and presents the definitions of normalized directivity we use in this paper.

## 2.0 Circular Polarization

As we will show, the radiated field of the COBRA antenna class exhibits circular polarization. Circular polarization is defined as [1]:

*“An electromagnetic wave for which either the electric or the magnetic field vector at a fixed point describes a circle at the rate of the wave frequency.”*

Furthermore, a circularly polarized wave will exhibit either left- or right-handed circular polarization (LHCP or RHCP) depending on the direction in which the electric or magnetic field describes the circle. Again, paraphrasing from [1]:

***Left-Handed Circular Polarization (LHCP)** - A circularly polarized electromagnetic wave in which the rotation of the electric field vector with time is counterclockwise for a stationary observer looking in the direction of the wave normal (or from the wave source). For an observer looking from a receiver toward the apparent source of the wave, the direction of rotation is reversed.*

Likewise:

***Right-Handed Circular Polarization (RHCP)** - A circularly polarized electromagnetic wave in which the rotation of the electric field vector with time is clockwise for a stationary observer looking in the direction of the wave normal (or from the wave source). For an observer looking from a receiver toward the apparent source of the wave, the direction of rotation is reversed.*

Figure 1 depicts the electric field distribution of a wave propagating in the +z-direction at a particular instant in time. The figure shows that the magnitude of the field is

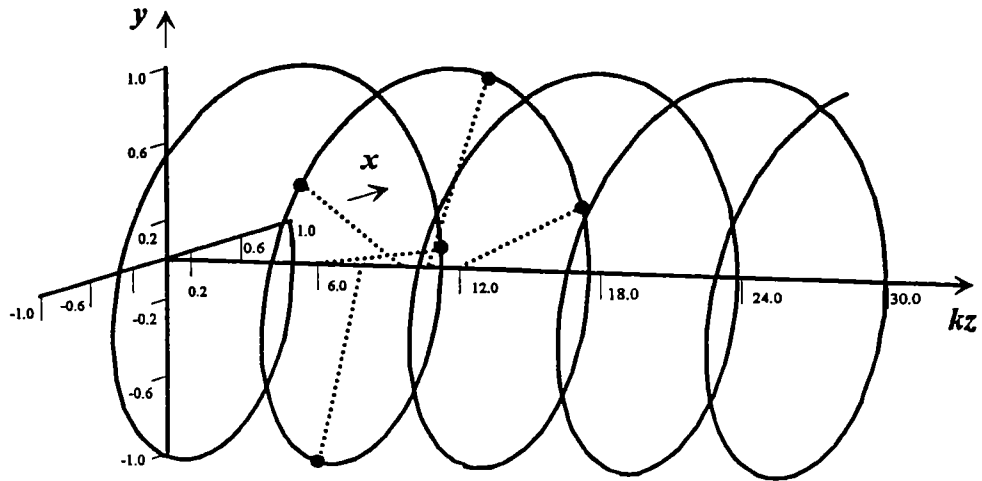


**Figure 1. A right-handed circularly polarized (RHCP) wave propagates in the  $+z$ -direction. Its magnitude is constant, but the direction is rotating with position as a left-handed helix.**

constant, but the direction is rotating with position. Shown in the figure is Right-Handed Circular Polarization (RHCP), which in space (not time) is a left-handed helix.

The mathematical form of the time-harmonic [2], plane TEM, circularly polarized wave that propagates in the z-direction can be expressed as:

$$\mathbf{E}(t,z) = \text{Re} \left[ E_0 \left( \mathbf{a}_x \mp j \mathbf{a}_y \right) e^{j(\omega t - kz)} \right], \quad (1)$$

which when evaluated at  $z = 0$  reduces to the following form

$$\mathbf{E}(t,z=0) = E_0 \left( \mathbf{a}_x \cos(\omega t) \pm \mathbf{a}_y \sin(\omega t) \right). \quad (2)$$

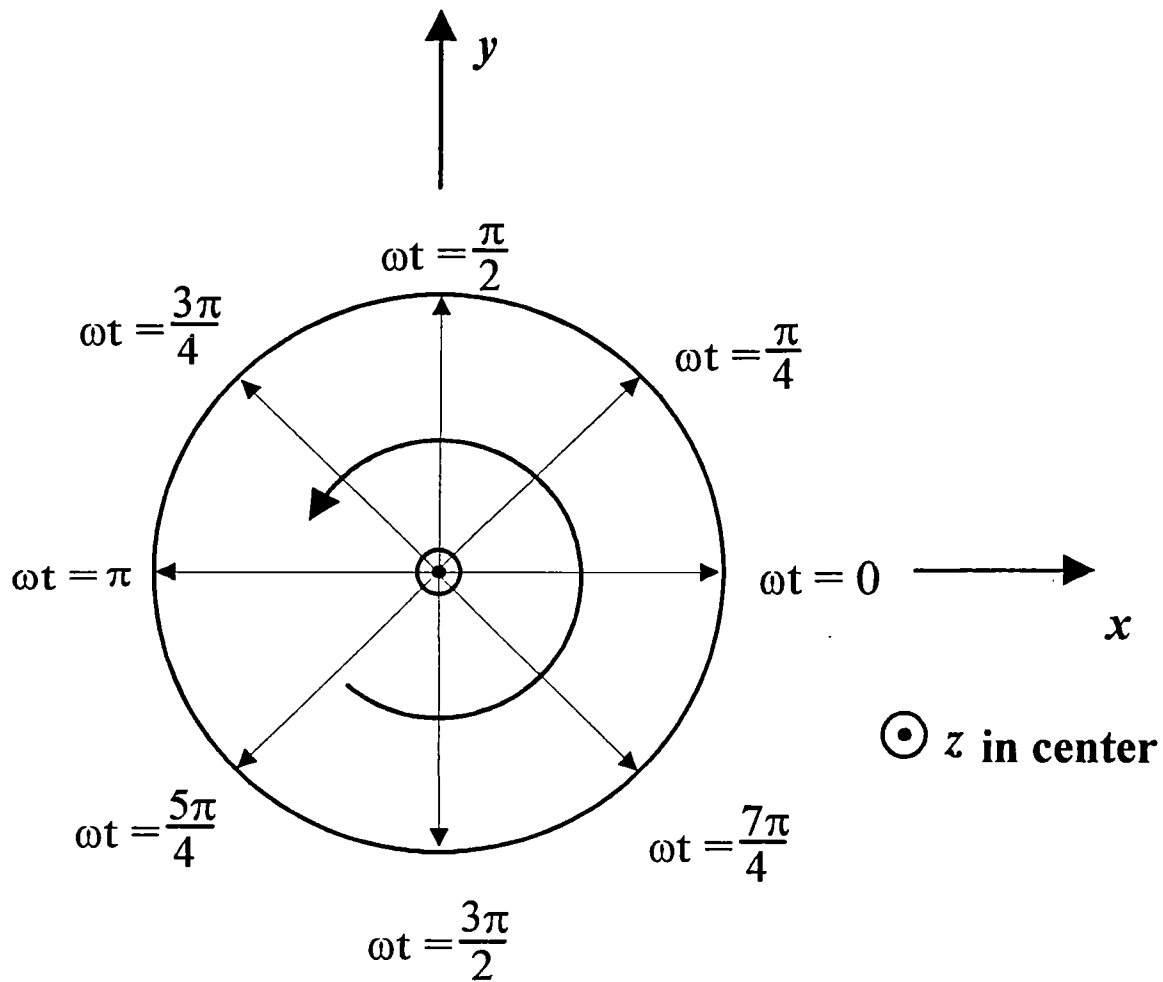
The upper sign is associated with RHCP, while the lower sign yields LHCP.

Table 1 relates the values of the components of the electric field given in Eqn. 2 at various instances of time for the two polarizations.

Figure 2 shows the rotation of the electric field vector as a function of time, and at a fixed location in space, for a RHCP wave. Note that the observation position is from a potential receiving site, and consequently the electric field vector rotates counterclockwise when viewed from this position.

**Table 1. Values of the components of the electric field given in Eqn. 2 at various instances of time for RHCP and LHCP.**

$\omega t = \frac{2\pi}{T}t$	RHCP $E_x$	RHCP $E_y$	LHCP $E_x$	LHCP $E_y$
0	$E_0$	0	$E_0$	0
$\pi/4$	$\frac{\sqrt{2}}{2}E_0$	$\frac{\sqrt{2}}{2}E_0$	$\frac{\sqrt{2}}{2}E_0$	$-\frac{\sqrt{2}}{2}E_0$
$\pi/2$	0	$E_0$	0	$-E_0$
$3\pi/4$	$-\frac{\sqrt{2}}{2}E_0$	$\frac{\sqrt{2}}{2}E_0$	$-\frac{\sqrt{2}}{2}E_0$	$-\frac{\sqrt{2}}{2}E_0$
$\pi$	$-E_0$	0	$-E_0$	0
$5\pi/4$	$-\frac{\sqrt{2}}{2}E_0$	$-\frac{\sqrt{2}}{2}E_0$	$-\frac{\sqrt{2}}{2}E_0$	$\frac{\sqrt{2}}{2}E_0$
$3\pi/2$	0	$-E_0$	0	$E_0$
$7\pi/4$	$\frac{\sqrt{2}}{2}E_0$	$-\frac{\sqrt{2}}{2}E_0$	$\frac{\sqrt{2}}{2}E_0$	$\frac{\sqrt{2}}{2}E_0$
$2\pi$	$E_0$	0	$E_0$	0



**Figure 2.** A RHCP plane wave is propagating along the z-direction. The arrow indicates the rotation direction of the electric field vector at various instances of time and at a fixed location in space. The observation position is from a potential receiving site, and consequently the electric field vector rotates counterclockwise from this perspective.

### 3.0 Fundamental Concept of COBRA Operation

The prior section discussed circular polarization, in this section we present some fundamental COBRA concepts, and show how the geometry of the antenna transforms an azimuthally symmetric mode distribution of a source into an aperture distribution that radiates a circularly polarized field with a boresight peak.

Figure 3 illustrates a paraboloidal reflector antenna fed by a conical horn antenna located with its phase center at the focal point of the reflector [6]. The conical horn is driven by the circular waveguide  $TM_{01}$  mode. As depicted in the figure, the conical horn radiates a doughnut-shaped pattern, which is characteristic of the driving mode. If the reflector were shaped conventionally, then the radiated pattern also would also exhibit a doughnut-shaped pattern with a null-on boresight. However, the surface of the paraboloidal reflector is divided into four quadrants (in general  $N$  sectors) and stepped as shown in Figure 3b. The reflector surface is "stepped" as indicated in the figure, so that each quadrant of the subreflector is displaced from a nominal position by an amount required to produce the proper phase shift in its incident field to produce the desired radiation characteristics (boresight peak pattern and circular polarization). The scattering from the reflector then produces a highly collimated, high-gain, on-axis beam with circular polarization. The following paragraphs discuss the concept for the particular case of a four step reflector driven by a conical feed horn antenna located at the focal point (see Figure 3a). Other geometries are discussed in later sections, and the derivation of the governing equations for the radiated field of a reflector with  $N$  steps is given in the appendix.

#### 3.1 Radiated Field of a 4 Step COBRA Aperture

For this COBRA example, the radiation characteristics of a four-quadrant reflector with discrete steps in the surface height between the equi-angular

quadrants is illustrated. We assume the incident field is  $E_p \mathbf{a}_p = E_0 \mathbf{a}_p$ , where  $E_0$  is the strength of the field. In Cartesian coordinates, the reflector incident field is  $E_x \mathbf{a}_x = E_0 \cos(\varphi) \mathbf{a}_x$ , and  $E_y \mathbf{a}_y = E_0 \sin(\varphi) \mathbf{a}_y$ . Due to the different path lengths from the reflector focus, to the the reflector surface and on to the aperture plane in front of the reflector surface, the steps in the reflector introduce a relative phase shift in the reflected field of the  $N = 4$  quadrants. Then:

1. Each quadrant is displaced from its opposing quadrant (I to III, and II to IV) such that there is a round-trip path length difference of  $\lambda / 2$  from the opposing quadrants. Because the fields in opposing quadrants were originally  $\pi$  out of phase, the path length difference between them brings the fields in quadrants I and III, and in quadrants II and IV into phase with each other.
2. Also, the linearly polarized field radiated by quadrants I and III lags by  $\pi/2$  in phase of the orthogonal field radiated by quadrants II and III. Consequently the aperture field radiates right hand circular polarization (RHCP).

**Stepped Paraboloidal  
Main Reflector**

$$\frac{F}{D} \cong 0.3 \text{ or } 0.4 \text{ (standard)}$$

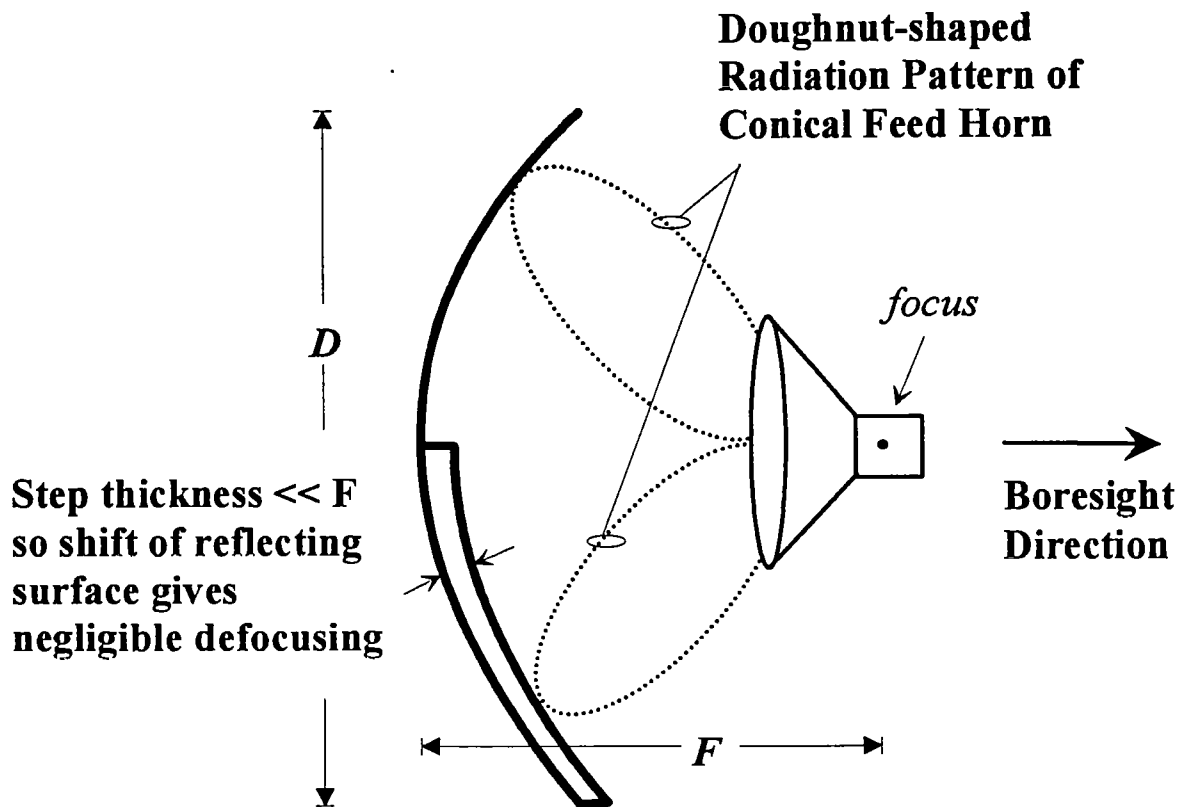


**Figure 3a.** The fundamental concept of the COBRA is shown: A paraboloidal reflector antenna is fed by a conical horn antenna located with its phase center at the feedpoint. The conical horn radiates the characteristic doughnut-shaped pattern of the  $TM_{01}$  mode, but the surface of the paraboloidal reflector is stepped to produce a circularly polarized radiated field with a bore-sight peak.

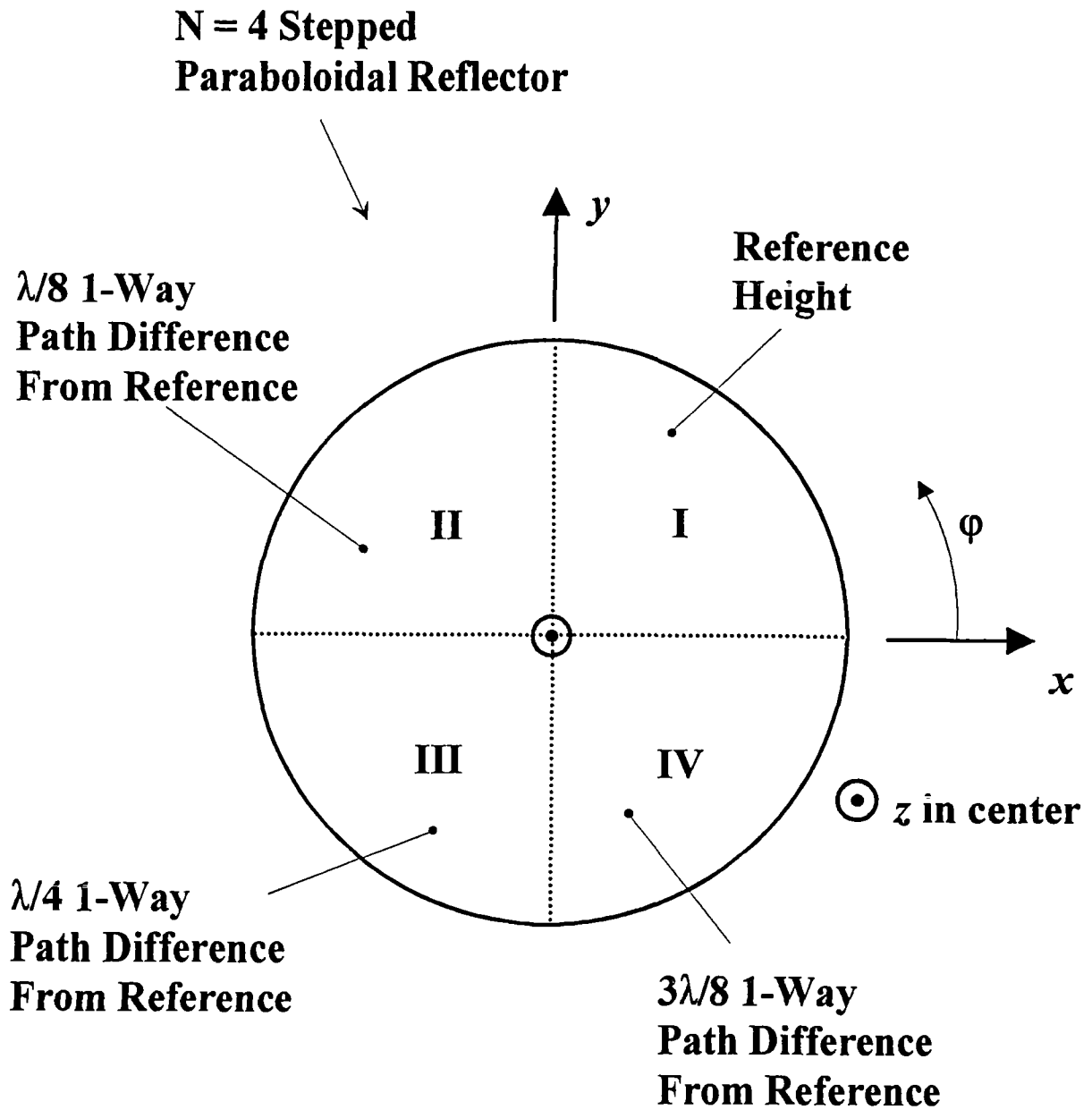


**Figure 3b.** The paraboloidal reflector surface is divided into four quadrants and stepped by increments of  $\lambda / 8$  to produce different path lengths to the aperture plane.

The boresight radiated field for the case  $N = 4$  is found using the results of the appendix. We write the far zone components of the electric vector potential on boresight as

$$F_x(N = 4) = E_0(\pi a^2) \frac{e^{-jkr}}{2\pi r} \xi_x(4) = E_0(\pi a^2) \frac{e^{-jkr}}{2\pi r} \left[ \frac{1}{\pi} \left( 1 - e^{-j\frac{\pi}{2}} \right) \right] \quad (3a)$$

and

$$F_y(N = 4) = E_0(\pi a^2) \frac{e^{-jkr}}{2\pi r} \xi_y(4) = E_0(\pi a^2) \frac{e^{-jkr}}{2\pi r} \left[ \frac{1}{j\pi} \left( 1 - e^{-j\frac{\pi}{2}} \right) \right] \quad (3b)$$

where  $a = D/2$  is the radius of the aperture. The boresight radiated field then is

$$\begin{aligned} \mathbf{E}(r) &= -j\omega\epsilon\eta \left[ \mathbf{a}_x(-F_y) + \mathbf{a}_y(F_x) \right] \\ &= -j\omega\epsilon\eta E_0(\pi a^2) \frac{e^{-jkr}}{2\pi r} \left( \frac{1 - e^{-j\frac{\pi}{2}}}{\pi} \right) \left[ \mathbf{a}_x \left( \frac{-1}{j} \right) + \mathbf{a}_y(1) \right] \\ &= E_0(a^2) \frac{e^{-j\left(kr + \frac{\pi}{4}\right)}}{\lambda r} (\sqrt{2}) \left[ \mathbf{a}_x - j\mathbf{a}_y \right] \end{aligned} \quad (4)$$

Equation (4) describes a *right-handed circularly polarized field*. Again drawing on the results of the appendix, the normalized linear gain (ratio of the gain of COBRA boresight power density in a single polarization to that of a uniformly filled, linearly polarized aperture) of the four-step reflector is  $d_L(N = 4) = \xi^2(4) = 0.203$ , which in dB is  $d_L(N = 4) = -6.93$  dB. The circularly polarized gain (ratio of the total boresight radiated power density gain of the COBRA aperture to that of a uniformly filled, linearly polarized aperture) is  $d_c(4) = 2\xi^2(4) = 0.405$ , or  $d_c(4) = -3.922$  dB.

The normalized gain of the circular aperture can be computed for an arbitrary number of reflector steps (see the appendix). The table below gives the boresight normalized linear and circular gains for several values of  $N$ .

**Table 2. Normalized directivity for the linear and circular polarizations of the COBRA aperture as a function of the number of steps  $N$ .**

$N$	$d_L(N)$ in dB	$d_C(N)$ in dB	Comment
1	$-\infty$	$-\infty$	Standard reflector gives boresight null
2	-3.92	-3.92	One step gives linear polarization
3	-7.67	-4.66	First case of circular polarization
4	-6.93	-3.92	Circular polarization
6	-6.43	-3.41	Circular polarization
8	-6.25	-3.23	Circular polarization
12	-6.12	-3.11	Circular polarization
16	-6.08	-3.07	Circular polarization
32	-6.03	-3.02	Circular polarization
$\infty$	-6.02	-3.01	Asymptotic directivity

The case  $N = 1$  is that of the standard reflector (with no steps), and the indicated directivity means it radiates a boresight null. For  $N = 2$ , the COBRA aperture radiates linear polarization with a boresight directivity of  $d_L = -3.92$  dB. The first incidence of circular polarization occurs for  $N = 3$ , and the aperture produces circular polarization for all  $N \geq 3$ . The circular directivity ( $d_C$ ) is always 3 dB higher than the linear directivity and means that the total power density in the circularly polarized wave is twice that of each linear polarization. As  $N \rightarrow \infty$  (the case of a smoothly varying surface profile, the normalized directivities approach asymptotic limits of  $d_C \xrightarrow{N \rightarrow \infty} -3.01$  dB, and  $d_L \xrightarrow{N \rightarrow \infty} -6.02$  dB.

### 3.2 Surface Geometry of the COBRA Reflector

To produce the radiated field described in the last section, the reflector transforms the incident field using steps in the surface profile of the reflector. This creates a fractional wavelength path length difference from the focal point to the aperture plane for the different quadrants. The change in the path length should be small compared with the focal length of the reflector to ensure defocusing will be minimal. However, a uniform step of the surface will not result a  $\frac{\pi}{4}$  one-way phase difference in the paths associated with diametrically opposed sectors. The surface profile of the step must be determined as follows.

Inspection of Figure 4a indicates that the step thickness is related to the sector number and the location from the apex ( $\rho = 0, \theta = 0^\circ$ ). To determine this dependence of the step thickness on position, consider the following. Let the origin be at the focus of the reflector, then  $\rho$  is the perpendicular distance from the axis (the line connecting the focus and the apex) to a point on the reflector surface, and  $\theta$  is the angle between the axis and the line connecting the origin and the surface point. Figure 4a illustrates these quantities.  $A$  is the length of the optical path in the presence of the step, while  $A'$  is the length in its absence. To achieve the proper phase relationship between opposite quadrants, the difference in path lengths should be

$$A' - A = \lambda / 2. \quad (5)$$

The unit vectors normal to the surfaces are indicated, and the angle of incidence = angle of reflection =  $\theta / 2$  from the surface normal. Now consider the expanded view shown in Figure 4b. The path length difference is indicated by the bold line in the figure. The thickness of the step, at the angle  $\theta$  then is given by

$$A' - A = \tau + l = \lambda / 2, \quad (6)$$

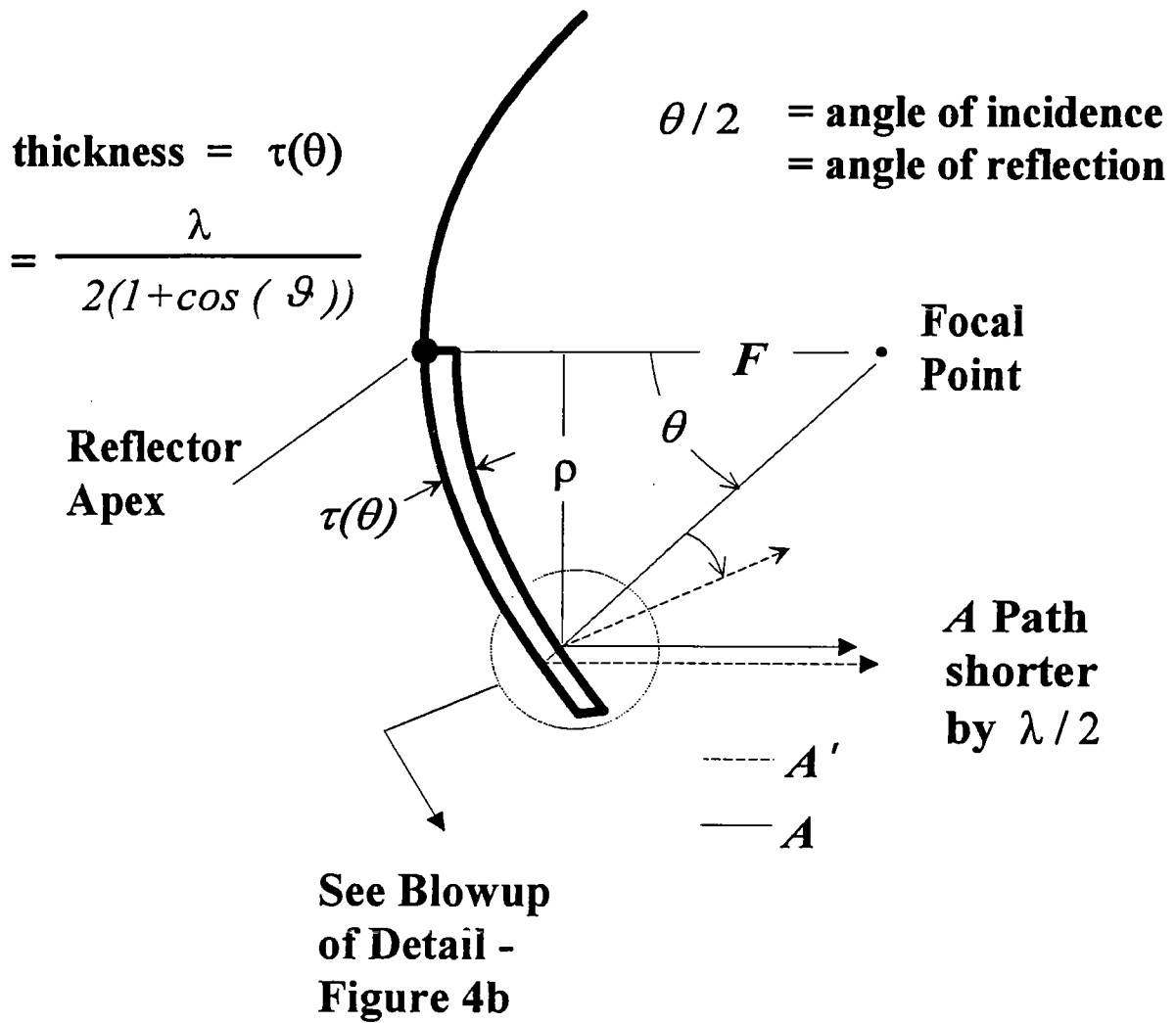
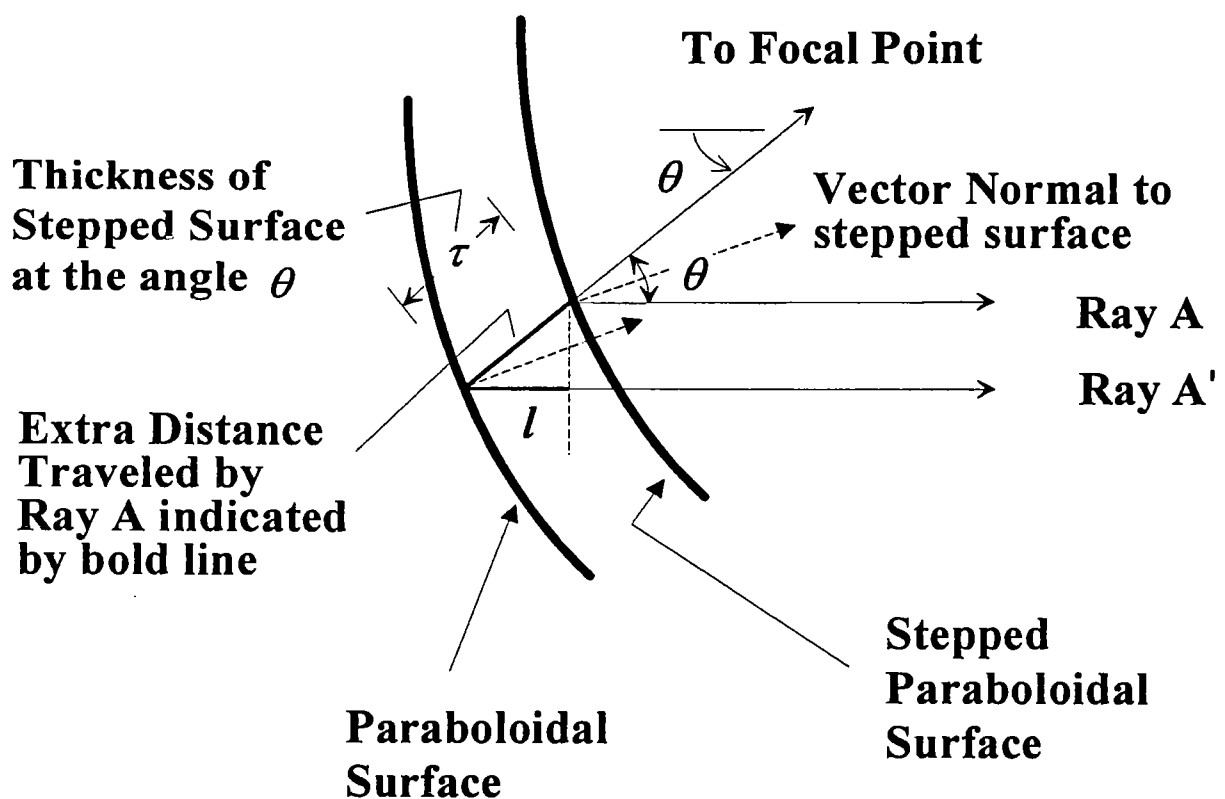


Figure 4a. Geometry of a COBRA reflector: coordinate origin is at the focus, and the angle  $\theta$  is measured from the axis of the reflector.



**Figure 4b. Geometry of a COBRA reflector: detail of the reflector surface used to help compute the thickness of the step as a function of the angle  $\theta$ .**

where  $l = \tau \cos(\theta)$ . Solving for the thickness

$$\tau = \frac{\lambda}{2(1 + \cos(\theta))} \quad (7)$$

A more convenient measure may be to specify the step thickness along the path of the vector normal to the paraboloidal surface at the angle  $\theta$ , for large reflectors this length approaches the value  $\tau \cos(\theta / 2)$ .

To demonstrate the dependence of the thickness  $\tau$  on angle, we consider a specific example. Operating at L-band (1 GHz), we have a 3 m (762 in.) diameter paraboloidal reflector with a 0.375 F/D ratio, and  $N = 4$  steps. The step thickness as a function of the angle  $\theta$ , for each quadrant ( I through IV ) is as given in Table 3 below for this case ( $N = 4$ ).

**Table 3. Reflector step thickness as a function of the angle  $\theta$ , for each quadrant (I through IV) for this case  $N = 4$ :  $f = 1$  GHz,  $D = 3$  m (762 in.), and  $F/D = 0.375$ .**

$\theta$	$\tau_I$	$\tau_{II} = \frac{\lambda}{4(1 + \cos(\theta))}$	$\tau_{III} = \frac{\lambda}{2(1 + \cos(\theta))}$	$\tau_{IV} = \frac{3\lambda}{4(1 + \cos(\theta))}$
0°	0.0 cm	3.75 cm	7.50 cm	11.25 cm
15°	0.0 cm	3.82 cm	7.63 cm	11.46 cm
30°	0.0 cm	4.02 cm	8.04 cm	12.06 cm
45°	0.0 cm	4.40 cm	8.79 cm	13.2 cm
60°	0.0 cm	5.00 cm	10.0 cm	15.00 cm
75°	0.0 cm	5.96 cm	11.92 cm	17.88 cm
90°	0.0 cm	7.50 cm	15.0 cm	22.50 cm

Note that the values for quadrants III, and IV are arrived at by modifying the right-hand side of (7); the round-trip path length difference (relative to Quadrant I) should

be  $\lambda / 4$  for the second quadrant,  $\lambda / 2$  for the third quadrant, and  $3\lambda / 4$  for the fourth quadrant. These values are consistent with the path difference indications in Figure 4b. In this example, the focal length is 112.5 cm, and the maximum angle is  $\theta_{\max} = 67.4^\circ$ . Therefore, the maximum step thickness, which occurs in Quadrant IV, is  $\tau_{\max} = 16.25$  cm, which is 14.44% of the focal length. When the maximum step size becomes a substantial percentage of the focal length of the antenna, defocusing of the radiated beam could result. A reflector with a higher F/D ratio or longer focal length should then be used.

#### **4.0 Other COBRA Geometries**

Section 3 demonstrated the fundamental concepts of the COBRA class of antennas. There, a single paraboloidal reflector was driven by a conical horn antenna located at its focal point. This may be an inconvenient geometry for many applications. This section describes a number of other geometries that utilize Cassegrain-type configurations of two reflectors with the subreflector driven by the radiated field of a horn, or driven directly by the center conductor of a coaxial transmission line. A good discussion and summary of the concepts of conventional Cassegrain antennas can be found in [7]. All of the antenna types discussed below transform an azimuthally symmetric excitation field into an aperture distribution of the form discussed in the previous section, and consequently the following are categorized as COBRA-type antennas as well.

#### **4.1 Horn-Fed Cassegrain Configuration**

A Cassegrain geometry is depicted in Figure 5a. There, a conical horn antenna is shown opening through the apex of the main reflector. The aperture field distribution of the horn is the  $TM_{01}$  mode, and it drives a stepped subreflector. The subreflector is stepped, but each sector is hyperboloidal in shape and reflects the incident field back to the main reflector. In addition, the stepped subreflector

transforms the incident field distribution to the desired COBRA aperture distribution required to produce circular polarization with a boresight peak.

A second Cassegrain configuration is shown in Figure 5b. There, instead of stepping the subreflector, the main reflector is stepped. The operating principles are of course similar to those of the antenna shown in Figure 5a.

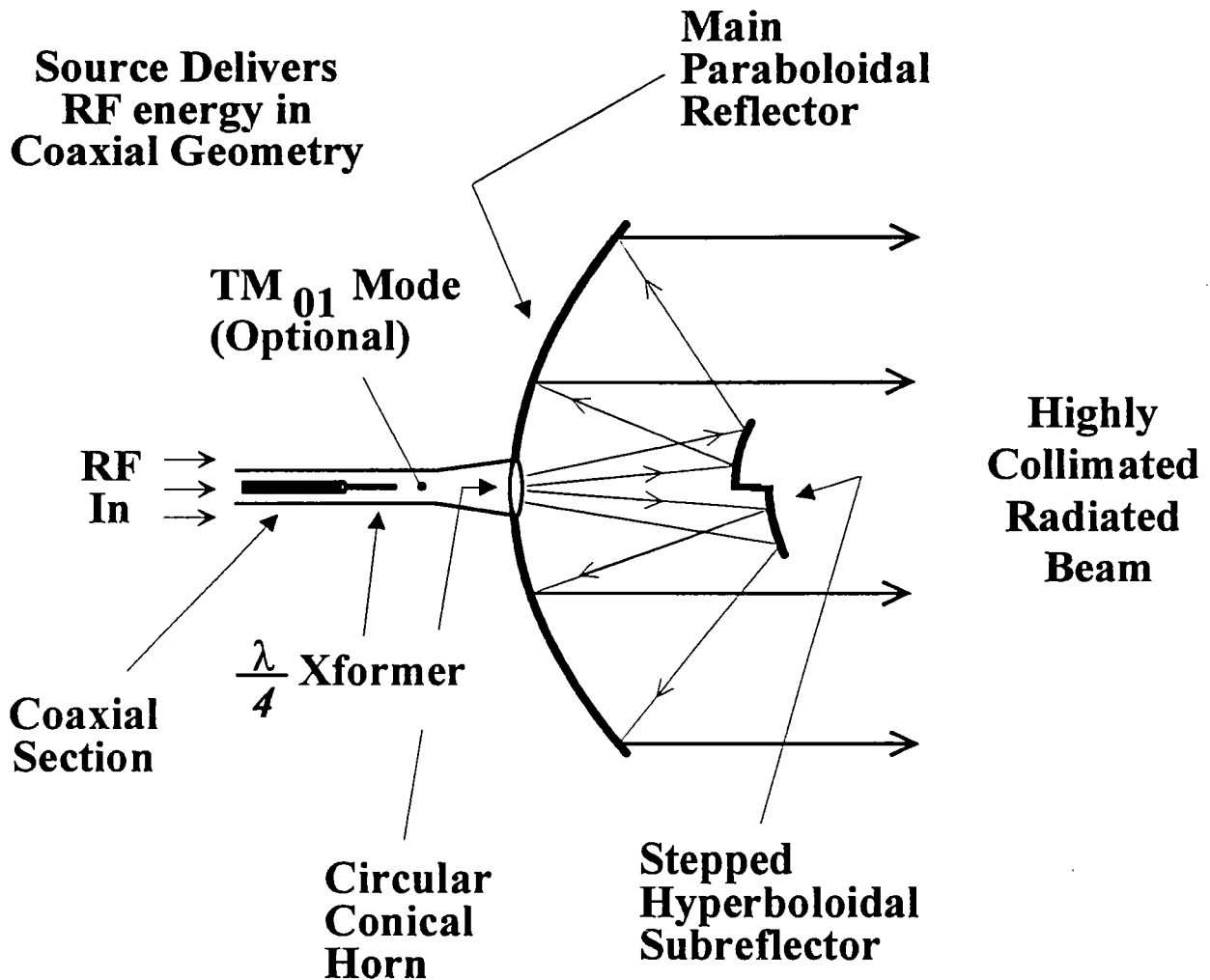
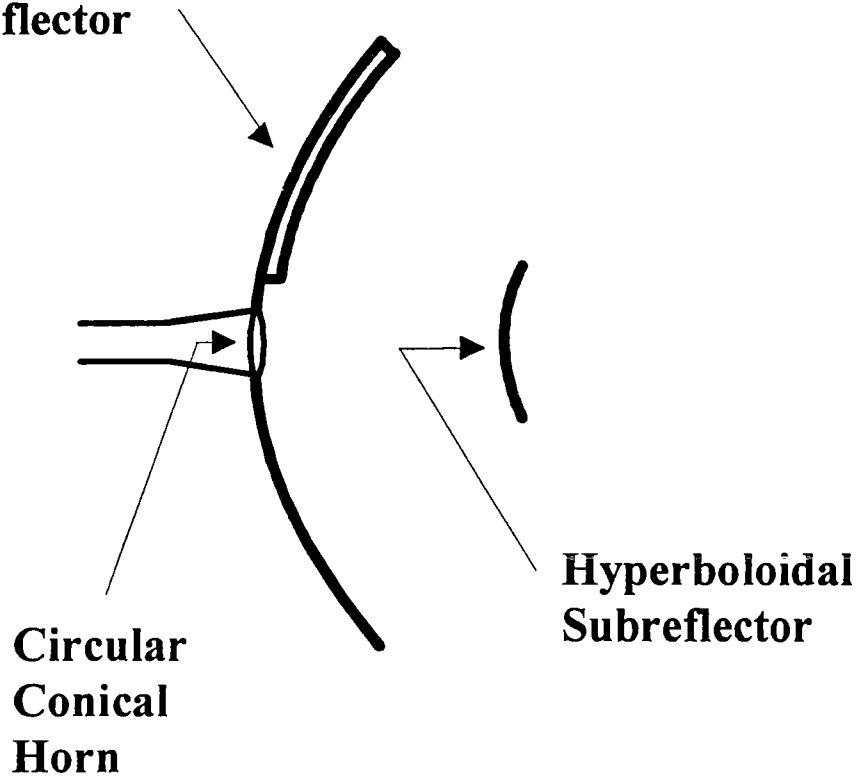


Figure 5a. COBRA antennas with the Cassegrain configuration: Stepped subreflector - the conical horn that opens through the apex of the main reflector drives the subreflector with a TM<sub>01</sub> circular waveguide mode; the subreflector transforms the incident field distribution and reflects the field onto the main reflector. The main reflector then produces the desired circular polarized radiated field with a boresight peak.

**Stepped Main  
Paraboloidal  
Reflector**



**Circular  
Conical  
Horn**

**Hyperboloidal  
Subreflector**

**Figure 5b. COBRA antennas with the Cassegrain configuration: Stepped main reflector - operates in a similar manner to the antenna shown in Figure 5a, but here the main reflector is stepped.**

## 4.2 Center Conductor-Fed Cassegrain Configuration

Many microwave sources develop the RF in a coaxial geometry in the TEM mode (also azimuthally symmetric in nature). One would like to avoid the mode conversion from coaxial TEM to circular  $TM_{01}$  as shown in Figure 5a, but the radiation efficiency for a simple truncated coaxial line is low. Another way to establish the desired aperture distribution is to continue the center conductor of the coaxial line through the apex of the main reflector and attach it directly to the subreflector. This idea is demonstrated in the antenna concepts depicted in Figures 6a and b. Rather than illuminating the subreflector via a radiated field, the subreflector is “driven” directly by the guided wave bound to the center conductor of the coaxial line. The subreflector scatters this field back toward the main reflector, and the stepped main reflector transforms the aperture field to the desired form.

Two forms are shown in Figure 6. The first simply extends the center conductor, preserving its circular cylindrical shape, out to the subreflector. The second form shown also extends the center conductor out to the subreflector, but the shape is tapered such that it becomes circular conical in nature. Each form may have certain desirable attributes. The incident wave propagating on the circular cylindrical conductor may bind more tightly to the conducting surface, and scatter off the subreflector less easily. However, the quasi-TEM nature of the guided wave on the center conductor may be well preserved. The second form, in which the geometry of the center conductor becomes circular conical, may not preserve the quasi-TEM form of the guided wave as well the first form, but this geometry may bind the wave to the center conductor less tightly, and consequently scatter from the subreflector to the main reflector more efficiently. Note that the subreflector can also be stepped for these cases, much in the manner depicted in Figure 5a.

The single reflector case also can be utilized. In that case the center conductor will exit the feed horn, which would be located in front of the reflector. The center conductor can be of the proper shape and length to provide the required illumination of the reflector, and / or dielectric lenses can be used to make the configuration more compact or efficient.

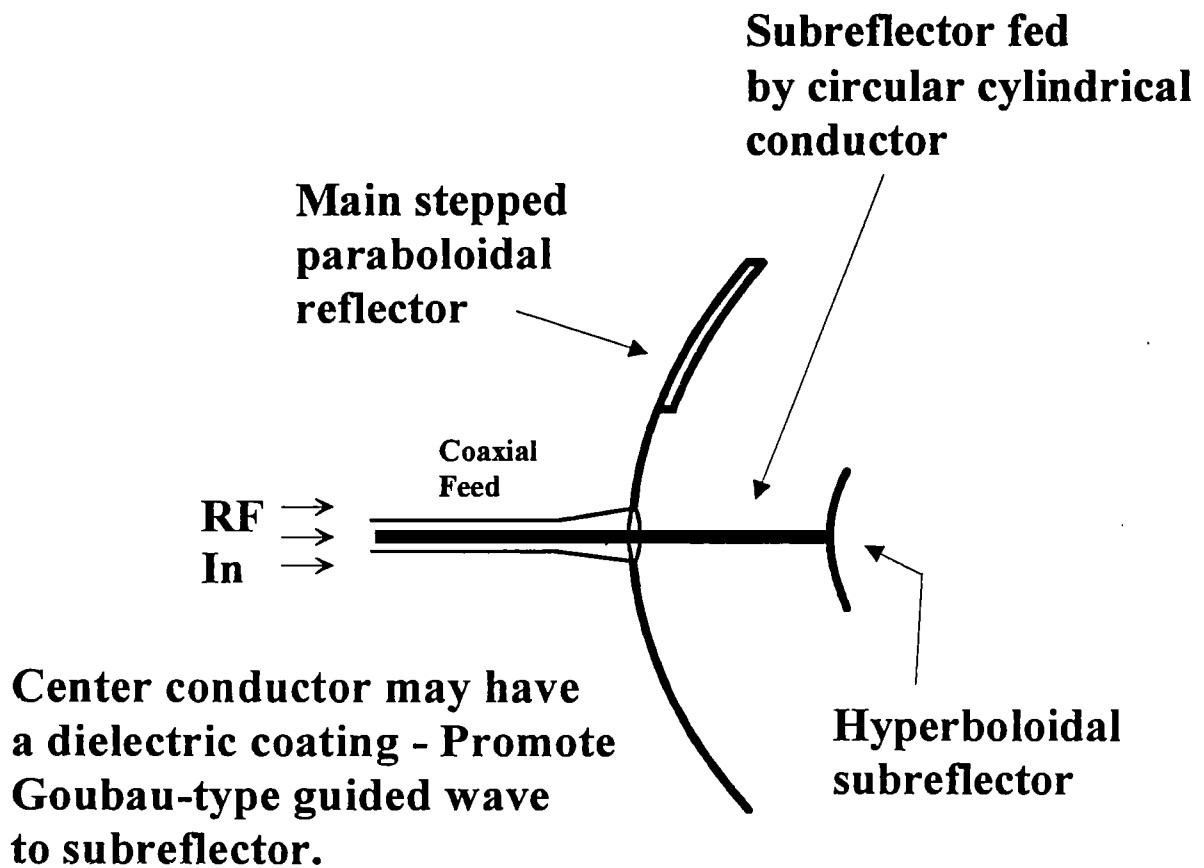


**Figure 6a.** COBRA antennas with the subreflector driven by the center conductor of a coaxial feed: the circular cylindrical center conductor is extended to the subreflector.

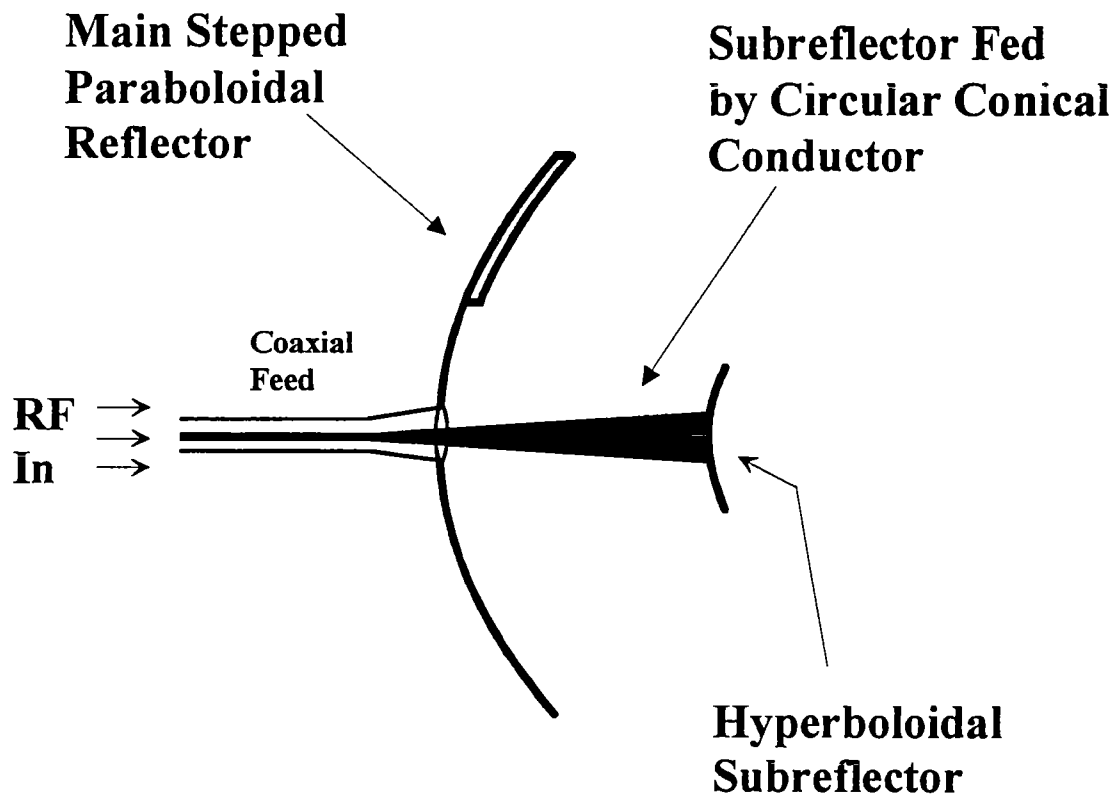


**Figure 6b.** COBRA antennas with the subreflector driven by the center conductor of a coaxial feed: the center conductor is shaped into a circular conical geometry and extended to the subreflector.

## 5. Concluding Remarks

This note has presented some of the fundamental concepts of a new class of reflector antennas. These antennas have been classified as the Coaxial Beam-Rotating Antennas, or COBRA, because they produce a radiated field that exhibits circular polarization. The discussion and analysis given here demonstrates the nature of the radiated field, and presents a number of possible antenna geometries that can be used to establish essentially the same aperture field distribution that yields the desired form of the radiated field.

A number of other types of geometries remain to be explored. These include: (1) Dielectric-coated center conductor - Instead of driving the subreflector with a bare conductor, the conductor is coated. This will help establish a guided surface wave [8, 9] that travels to the subreflector closely bound to the conductor. (2) The use of dielectric stepped reflectors - The use of perfect electric conductor (PEC) steps dictates free space propagation to establish the required path length differences for the quadrants. However, for some cases the step heights required may be a significant portion of the focal length and could defocus the boresight beam. The use of stepped dielectric coatings could serve the same function as the stepped PEC, but would require smaller step sizes. The defocusing could be less severe. (3) Lenses - Dielectric lenses have been used as focusing elements and antennas for some time. Familiar examples include Luneburg [10] and Fresnel Lenses [11]. A lens also could be used to condition the field from a horn antenna to radiate circular polarization directly, or to drive a reflector. This would obviate the need to step the surface height of the reflector surface. Many other antenna geometries can be considered as well.

Additional work is required to better analyze the radiated field of the COBRA class of antenna. Effort will include: analysis of the effect of subreflector aperture blockage; total pattern calculations; and the rigorous analysis of the center conductor-driven subreflector geometries. Also, the

design, fabrication and measurement of a COBRA prototype would be useful to validate the analysis presented here.

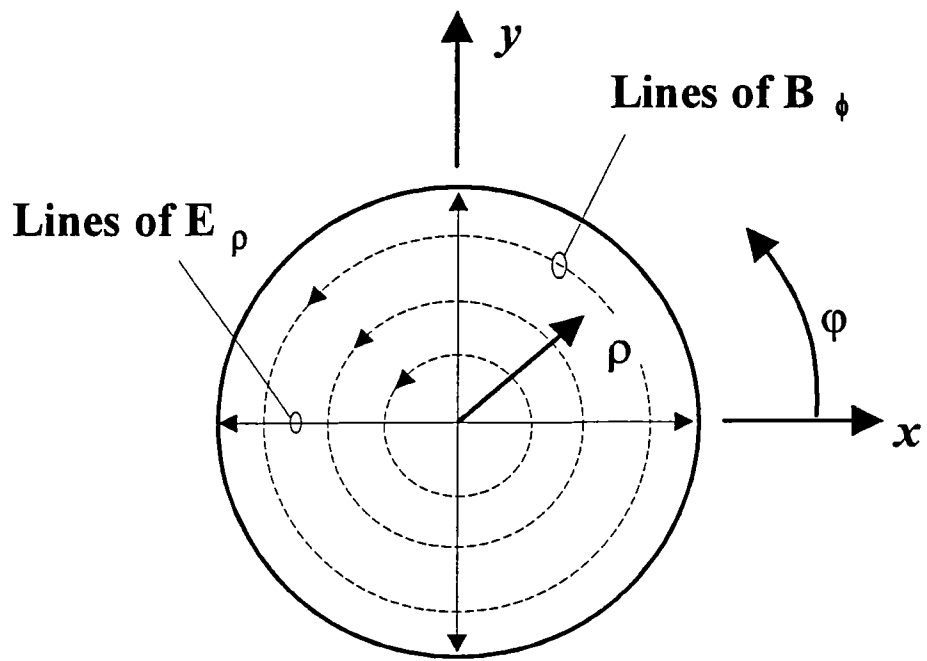


**Figure A1.** Feed horn aperture distribution, which also is the form of the main reflector incident field. Assume the magnitude of the E-field is independent of position.

incident on the main reflector is then similar to the horn aperture distribution shown in Figure A.1.

We can write this incident field in cylindrical coordinates as  $E_\rho \mathbf{a}_\rho = E_0 \mathbf{a}_\rho$ , where  $E_0$  is the strength of the field. In Cartesian coordinates, this is  $E_x \mathbf{a}_x = E_0 \cos(\varphi) \mathbf{a}_x$ , and  $E_y \mathbf{a}_y = E_0 \sin(\varphi) \mathbf{a}_y$ . This incident field illuminates the stepped main reflector, which in turn introduces a relative phase shift in the reflected field among the  $N$  sectors. Then, accounting for the amount of relative displacement of the stepped reflector surface, the projected antenna aperture field can be written as

$$E_y^A = E_0 \sin(\varphi) e^{j\psi(\varphi)} \quad (\text{A.1})$$

and

$$E_x^A = E_0 \cos(\varphi) e^{j\psi(\varphi)}, \quad (\text{A.2})$$

where the phase  $\psi(\varphi)$ , is dependent on the round-trip distance from the feed horn, to the reflector surface, and back to the antenna aperture plane; it is a function of the variable  $\varphi$ . This (non-physical) aperture field has been approximated with the following assumptions:

1. The illumination of the reflector is uniform in magnitude,  $\rho$ -directed, and not dependent on the feed horn pattern;
2. Feed horn, to reflector surface, to antenna aperture path length differences are not important - no  $1/r$  variation in the field;
3. Aperture blockage effects are negligible; and
4. Diffraction effects are not important.

Now assume that the reflector has a diameter  $D = 2a$  and is stepped in  $N$  equal-angle sections. For  $\frac{2\pi(n-1)}{N} = \varphi_{n-1} \leq \varphi \leq \varphi_n = \frac{2\pi n}{N}$ , we let

$$\psi(\varphi) = \frac{2\pi(n-1)}{N} \text{ for } n = 1, 2, \dots, N. \quad (\text{A.3})$$

This corresponds to a counter-clockwise increase in the step thickness on the reflector. We show later that for  $N \geq 3$ , the counter-clockwise (positive  $z$  normal to the reflecting surface at the apex) step size increase yields RHCP, while a clockwise step size increase yields LHCP. In spherical coordinates the radiated electric field can be expressed in terms of the electric vector potential [3] as

$$\mathbf{E}(\mathbf{r}) = j\omega\epsilon\eta \mathbf{a}_r \times \mathbf{F}(\mathbf{r}) \quad (\text{A.4})$$

where

$$\mathbf{F}(\mathbf{r}) = \frac{e^{-jkr}}{4\pi r} \int_{S_i} 2 \left( [\mathbf{E}^A(\varphi') \times \hat{\mathbf{n}}] \right) e^{jk_x x + jk_y y} ds', \quad (\text{A.5})$$

$k_x = k \sin(\vartheta) \cos(\varphi)$  and  $k_y = k \sin(\vartheta) \sin(\varphi)$ , and  $\eta = \sqrt{\frac{\mu}{\epsilon}}$  is the intrinsic wave impedance of the medium. The components of the radiated electric vector potential can be computed in terms of the aperture distribution, they are:

$$\begin{aligned} F_x = \mathbf{F} \cdot \mathbf{a}_x &= \frac{e^{-jkr}}{4\pi r} \int_{S_i} 2 \left( [\mathbf{E}^A(\varphi') \times \hat{\mathbf{n}}] \cdot \hat{\mathbf{a}}_x \right) e^{jk_x x + jk_y y} ds' \\ &= \frac{e^{-jkr}}{2\pi r} \int_0^{2\pi} \int_0^a E_x(\varphi') e^{jk \rho' \sin \vartheta \cos(\varphi - \varphi')} \rho' d\rho' d\varphi, \quad (\text{A.6a}) \\ &= \frac{e^{-jkr}}{2\pi r} \int_0^{2\pi} \int_0^a E_0 \sin(\varphi') e^{j\psi(\varphi')} e^{jk \rho' \sin \vartheta \cos(\varphi - \varphi')} \rho' d\rho' d\varphi' \end{aligned}$$

and similarly

$$F_y = \mathbf{F} \cdot \mathbf{a}_y = \frac{e^{-jkr}}{2\pi r} \int_0^{2\pi} \int_0^a E_0 \cos(\varphi') e^{j\psi(\varphi')} e^{jk \rho' \sin \vartheta \cos(\varphi - \varphi')} \rho' d\rho' d\varphi'. \quad (\text{A.6b})$$

With the expression for  $\psi(\varphi)$  given above, the components can be expressed as

$$F_x = E_0 \frac{e^{-jkr}}{2\pi r} \sum_{n=1}^N e^{j\frac{2\pi(n-1)}{N}\varphi_n} \int_{\varphi_{n-1}}^{\varphi_n} \int_0^a \sin(\varphi') e^{jk \rho' \sin \vartheta \cos(\varphi - \varphi')} \rho' d\rho' d\varphi' \quad (\text{A.7a})$$

and

$$F_x = E_0 \frac{e^{-jkr}}{2\pi r} \sum_{n=1}^N e^{j\frac{2\pi(n-1)}{N}\varphi_n} \int_{\varphi_{n-1}}^a \int_0^a \cos(\varphi') e^{jk\rho' \sin\vartheta \cos(\varphi-\varphi')} \rho' d\rho' d\varphi'. \quad (\text{A.7b})$$

The above, when properly evaluated will yield the complete radiated pattern of the COBRA aperture.

The expressions can be simplified considerably if one wishes to compute the boresight field only ( $\vartheta = 0, \varphi = 0$ ). For that case, the integrals are easily evaluated, and the potential components written as

$$F_x = E_0 (\pi a^2) \frac{e^{-jkr}}{2\pi r} \xi_x(N) \quad (\text{A.8a})$$

and

$$F_y = E_0 (\pi a^2) \frac{e^{-jkr}}{2\pi r} \xi_y(N). \quad (\text{A.8b})$$

where the factors  $\xi_x(N)$  and  $\xi_y(N)$ , which are functions of the number of steps in the reflector, are

$$\xi_x(N) = \frac{1}{2\pi} \sum_{n=1}^N e^{j\frac{2\pi(n-1)}{N}} (\cos(\varphi_{n-1}) - \cos(\varphi_n)) \quad (\text{A.9a})$$

and

$$\xi_y(N) = \frac{1}{2\pi} \sum_{n=1}^N e^{j\frac{2\pi(n-1)}{N}} (\sin(\varphi_n) - \sin(\varphi_{n-1})). \quad (\text{A.9b})$$

The above expressions can be written in closed form without the summations. One writes the  $\sin(-)$  and  $\cos(-)$  terms as exponentials

$$\xi_x(N) = \frac{1}{2\pi} \sum_{n=1}^N e^{j\frac{2\pi(n-1)}{N}} \left( \frac{e^{j\varphi_{n-1}} + e^{-j\varphi_{n-1}}}{2} - \frac{e^{j\varphi_n} + e^{-j\varphi_n}}{2} \right), \quad (\text{A.10})$$

substitute for  $\varphi_{n-1}$  and  $\varphi_n$ , and group like terms to obtain

$$\xi_x(N) = \frac{1}{4\pi} \sum_{n=1}^N \left\{ \left( 1 - e^{-j\frac{2\pi}{N}} \right) + \left( e^{-j\frac{4\pi}{N}} - e^{-j\frac{2\pi}{N}} \right) e^{j\frac{4\pi n}{N}} \right\}. \quad (\text{A.11})$$

Then one uses the properties of a finite geometric progression [15] to get the following forms:

$$\xi_x(N) = \begin{cases} 0 & , N = 1 \\ 2/\pi & , N = 2 \\ \xi(N) e^{-j\pi\left(\frac{2-N}{2N}\right)} & , N \geq 3 \end{cases} \quad (\text{A.12a})$$

and

$$\xi_y(N) = \begin{cases} 0 & , N = 1 \\ 0 & , N = 2 \\ \xi(N) e^{-j\frac{\pi}{N}} & , N \geq 3, \end{cases} \quad (\text{A.12b})$$

where the term which gives the magnitude is

$$\xi(N) = \frac{N}{2\pi} \sin\left(\frac{\pi}{N}\right). \quad (\text{A.12c})$$

Note that one must evaluate explicitly the first two terms ( $N = 1$  and  $N = 2$ ) using (A.11). Equations (A.8) and (A.10) describe the boresight radiated field for the case in which the reflector step thickness increases in the counter-clockwise direction.

By converting to the time domain, one can show this to be RHCP for all cases where  $N \geq 3$ . Note that the  $N = 1$  case represents an ordinary reflector and produces a null-on boresight, while the  $N = 2$  case produces linear polarization on boresight.

To achieve LHCP one would adjust the reflector surface step distribution such that  $\psi(\varphi) = \frac{2\pi(1-n)}{N}$ , for  $\frac{2\pi(1-n)}{N} = \varphi_{n-1} \leq \varphi \leq \varphi_n = \frac{-2\pi n}{N}$ ; this would give a discrete clockwise increase in the step thickness. For this case, it can be shown that

$$\xi_x^{LHCP}(N) = \begin{cases} 0 & , N = 1 \\ 2/\pi & , N = 2 \\ \xi(N) e^{j\pi\left(\frac{2-N}{2N}\right)} & , N \geq 3 \end{cases} \quad (\text{A.13a})$$

and

$$\xi_y^{LHCP}(N) = \begin{cases} 0 & , N = 1 \\ 0 & , N = 2 \\ \xi(N) e^{j\pi\left(\frac{1-N}{N}\right)} & , N \geq 3. \end{cases} \quad (\text{A.13b})$$

As before, we will observe that for  $N \geq 3$  the components are equal in magnitude, and in phase quadrature.

### Directivity of a Linearly Polarized Uniformly Filled Aperture

The radiated far-field of a linearly polarized, uniformly filled aperture is chosen as the standard by which we characterize the COBRA aperture. We let the aperture field

$$E_y^A \mathbf{a}_y = E_0 \mathbf{a}_y \quad (\text{A.14})$$

uniformly fill a circular aperture of radius  $a$ . The boresight radiated electric vector potential is then simply

$$F_y^U = E_0 (\pi a^2) \frac{e^{-jk r}}{2\pi r} = E_0 \left( D_U \frac{\lambda^2}{4\pi} \right) \frac{e^{-jk r}}{2\pi r} \quad (\text{A.15})$$

where the directivity of the uniformly filled aperture is well known to be

$$D_U = \frac{4\pi A}{\lambda^2} = \frac{4\pi(\pi a^2)}{\lambda^2}. \quad (\text{A.16})$$

### Directivity of the COBRA Aperture

It has been shown that the radiated field of the COBRA aperture exhibits circular polarization. When referenced to the radiated field of a uniformly filled aperture, one can choose to weigh the ratio of power density in one of the linear components of the circularly polarized field, or compare the total power that is the sum of the powers in each polarization. We make the following definition.

$D_L$  = absolute linear directivity of the COBRA aperture

For example, referenced to the x-component of the boresight field, the directivity is

$$D_L = \frac{1}{2} \frac{|E_x(R)|^2}{\eta} \left( \frac{4\pi R^2}{P^{Rad}} \right) \quad (\text{A.17})$$

where  $P^{Rad}$  = total radiated power. Also,

$D_C$  = directivity the COBRA aperture based on total power density

Then,

$$D_C = \frac{1}{2} \frac{|E_x(R)|^2 + |E_y(R)|^2}{\eta} \left( \frac{4\pi R^2}{P^{Rad}} \right) \quad (\text{A.18})$$

where  $P^{Rad} = \frac{1}{2} \frac{E_0^2}{\eta}$  is the total radiated power of the aperture. These values can be

normalized to the directivity of a uniformly filled aperture; we define the normalized directivity figures of merit to be

$$d_L = \frac{D_L}{D_U} = \xi^2(N) \quad (\text{A.19})$$

and

$$d_C = \frac{D_C}{D_U} = 2\xi^2(N) \quad (\text{A.20})$$

for  $N \geq 3$  on boresight. The last relations are found simply by forming the ratios indicated, then substitution for the indicated quantities, and reduction to simplest form.

## References

1. *IEEE Standard Definitions of Terms for Radio Wave Propagation*, IEEE Std 211-1977, Institute of Electrical and Electronics Engineers, Inc., 345 East 47<sup>th</sup> St., NY, 10017.
2. R. Harrington, *Time Harmonic Electromagnetic Fields*, McGraw-Hill, New York, 1961, ISBN 07-026745-6.
3. W. Stutzman and G. Thiele, *Antenna Theory and Design*, John Wiley and Sons, New York 1981, ISBN 0-471-04458-X.
4. R. Collin, *Antennas and Radiowave Propagation*, McGraw-Hill, New York, 1985, ISBN 0-07-011808-6.
5. C. E. Baum and H. N. Kritikos, Symmetry in Electromagnetics, Chapter 1 in C. E. Baum and H. Kritikos (eds.), *Electromagnetic Symmetry*, Taylor and Francis, 1995.
6. A. D. Olver, P. J. B. Clarricoats, A. A. Kishk, and L. Shafai, *Microwave Horns and Feeds*, IEEE Electromagnetic Waves Series 39, IEEE Press, New York, 1994, ISBN 0-85296-809-4.
7. P. E. Hannan, "Microwave Antennas Derived from the Cassegrain Telescope," IRE Trans. on Ant. and Prop., pp. 140 - 153, March, 1961.
8. R. E. Collin, *Field Theory of Guided Waves*, IEEE Press, New York, 1991, ISBN 0-87942-237-8.
9. G. Goubau, "Single conductor surface wave transmission lines," Proc. IRE vol. 39, pp. 619-624, June 1951.
10. T. Milligan, *Modern Antenna Design*, McGraw-Hill, Inc., NY, ISBN 0-07-042318-0, 1985.
11. Y. T. Lo and S. W. Lee, *Antenna Handbook*, (eds.), Van Nostrand Reinhold, NY, ISBN 0-442-25843-7, 1988.
12. W. Smythe, *Static and Dynamic Electricity*, Hemisphere Publishing Corp., (Taylor and Francis), New York, ISBN 0-89116-916-4, 1989.
13. C. E. Baum, "Focused Aperture Antennas," Sensor and Simulation Note 306, 19 May 1987.
14. C. E. Baum, "Radiation of Impulse-Like Transient Fields," Sensor and Simulation Note 321, November 1989.
15. M. Abramowitz and I. Stegun, *Handbook of Mathematical Functions*, pg. 10, eqn. 3.1.10, Dover Publications, Inc., NY, 1965, ISBN 0-486-61272-4.